Accurate quantification of phosphorus intergranular segregation in iron by STEM-EDX

Chih-Ying Hsu, J. Stodolna, P. Todeschini, F. Delabrouille, Bertrand Radiguet, Frédéric Christien

Accurate quantification of phosphorus intergranular segregation in iron by STEM-EDX

C.-Y. Hsu[1,2], J. Stodolna[1], P. Todeschini[1], F. Delabrouille[1], B. Radiguet[3], F. Christien[2]

1: EDF R&D, MMC Department, F-77250 Ecuelles, France

2: Mines Saint-Etienne, Univ Lyon, CNRS, UMR 5307 LGF, Centre SMS, F-42023 Saint-Etienne, France

3: Normandie Université, UNIROUEN, INSA Rouen, CNRS, Groupe de Physique des Matériaux, 76000 Rouen, France

---

Keywords: *Scanning transmission electron microscopy, energy dispersive X-ray spectroscopy, quantification, intergranular segregation, phosphorus, grain boundary*

Abstract

This study describes a method to quantify phosphorus grain boundary segregation by Energy Dispersive X-ray Spectroscopy in Scanning Transmission Electron Microscope (STEM-EDX). A "box-type method" is employed, removing the long-discussed problems of interaction volume and the beam broadening effect. The proposed methodology also introduces a novel way of subtracting the spectrum background to remove the influence of coherent Bremsstrahlung and spurious peaks. A Fe-P model alloy was used to compare the box method to the quantification results previously obtained by atom probe tomography on two high angle grain boundaries. The results are specifically reported in surface concentration (atom/nm^2) to avoid additional hypotheses and allow the results between the two techniques to be directly compared. The measurements show that the box-type method can accurately measure phosphorus intergranular segregation in iron.

1. Introduction

Intergranular segregation describes the rearrangement of solute atoms locally at the grain boundary. The most common grain boundary segregation identification and quantification technique is Auger Electron Spectroscopy (AES). The analyzable areas are limited to intergranular fracture surfaces [1] induced by grain boundary embrittlement. This implies that all surfaces analyzed by AES have a minimum quantity of segregated embrittling elements resulting in the possible occurrence of intergranular fracture. In addition, its high surface contamination sensitivity requires samples to be fractured in the ultra-high vacuum chamber, requiring specific equipment. In cases where intergranular fracture of the specimen cannot be achieved, analysis of the grain boundaries using AES is impossible, which is a strong limitation for this technique. Other techniques, such as Atom Probe Tomography (APT), have also been used to study segregation, especially when intergranular fracture is not seen [2], [3].

Different studies [4]–[10] have described the use of Scanning Transmission Electron Microscope equipped with Energy X-ray Dispersive Spectroscopy (STEM-EDX) to analyze intergranular segregation. Common issues for STEM-EDX intergranular segregation quantification are the interaction volume and the beam broadening effect [4], [11]. The signal contains information from the entire analyzed volume, including the matrix and the GB. The usual quantification procedures require information on beam size, electron distribution, and sample geometry, where some assumptions are necessary.

The results of “intergranular segregation amount” can be presented in different units, such as fraction of a monolayer [12], atomic percentage [13], [14], and surface concentration (atom/unit surface) [4]. Some of these units require assumptions that are rarely verified. For example, defining a fraction of a monolayer requires a hypothesis of thecrystallography (Miller indices) of

the segregated plane. As such, it is practically impossible to compare intergranular segregation quantification results from different sources.

Phosphorus intergranular segregation is a common phenomenon in low alloy steels during the manufacturing process or thermal ageing. It has been shown that, under certain conditions, phosphorus intergranular segregation decreases fracture properties [15]–[20]. Various studies used STEM-EDX to measure phosphorus intergranular segregation in low alloy steels. Some [13], [14], [21] used the spot method which involves positioning the electron beam on a well aligned grain boundary; others [22] proposed a line profile crossing the grain boundary from one adjacent grain to the next. Both approaches require beam size assumptions to resolve the beam broadening effect, allowing the apparent phosphorus concentration to be expressed as a concentration on the grain boundary. Their results showed that the phosphorus grain boundary segregation level can be very low (a few at%) after thermal ageing, meaning that the phosphorus signal to noise ratio is expected to be small. Furthermore, the position of the phosphorus Kα peak (2.01 keV) is within the range where coherent Bremsstrahlung [23] can occur and where possible spurious peaks with similar energy, such as Pt M and Zr L peaks [24], can be present. The background subtraction for the phosphorus peak is thus more complex than for other alloying elements.

The objective of this work is to develop a methodology to quantify phosphorus intergranular segregation by STEM-EDX without being influenced by an assumption on the interaction volume. This idea is similar to the raster scans proposed by others authors [4], [6]. Monte-Carlo simulations of X-ray emissions in thin foil were conducted to validate the “box-type” methodology. In this study, the quantification results are expressed as an interface concentration in atoms/nm², the definition of which is unambiguous and allows the results to be compared with quantifications from other methods. In addition, particular attention was paid to the method used to extract peak

intensity (background subtraction) as the phosphorus peak intensity is low and some spurious peaks interact with the phosphorus signal. Finally, the measurement accuracy was estimated and the questions of specimen ageing during storage and specimen damage due to electron beam were discussed. This work was conducted on two high angle grain boundaries of a Fe-P model alloy and the STEM-EDX quantification results were compared with previously published measurements obtained on the same grain boundaries using APT [2].

2. Material and methodology

The sample used consisted of a high purity Fe-0.034 at% P-0.01 at% C model alloy that was annealed at 650°C for 24 hours to induce phosphorus intergranular segregation. This same sample was studied by Akhatova et al. [2] where two high angle grain boundaries, named A1 and A2, were analyzed by APT. An orientation map of the microstructure and the positions of A1 and A2 grain boundaries are shown Figure 1(a) [25]. The lengths of A1 and A2 grain boundaries exceed a few hundred microns, leaving enough space to prepare thin foils by Focus Ion Beam (FIB) on the same grain boundaries. The grain boundaries were fully analyzed in [2] where information, including the rotation axes and the grain boundary planes, is provided.

It can be seen in Figure 1(b) that the A2 grain boundary is fairly straight and long for extraction of both APT tips and TEM thin foil samples. There were four preparation sites for APT tips and the TEM thin foil was extracted beside these sites. The thin foil was prepared using FEI Helios DualBeam FIB operating at 30 kV. The current used for final milling ranged from 920 nA to 28 nA. The grain boundary was positioned roughly at the center of the thin foil for easy recognition and the final thickness of the thin foil measured approximately 100 nm. Figure 1(c) shows a High Angle Annular Dark Field (HAADF) image of the A2 thin foil. It can clearly be seen that the grain boundary

is straight and located close to the center. Another TEM thin foil was prepared at A1 grain boundary in the same manner. The time interval between thin foil preparation and STEM-EDX analysis was no longer than 2 days, except for one particular case as explained later.

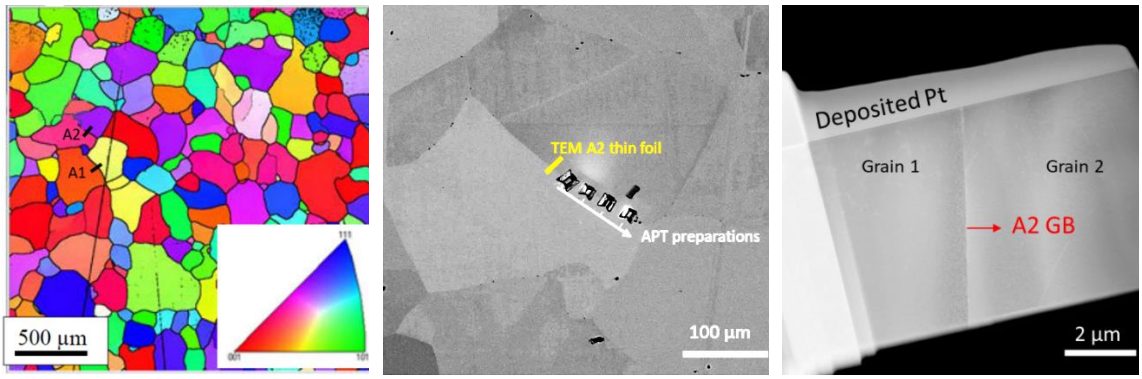

(a) (b) (c)

Figure 1. TEM thin foil preparation from the Fe-P model alloy, (a) inverse pole figure of the full sample surface, grain boundaries A1 and A2 were originally analyzed by APT in [25], (b) Scanning electron microscope micrograph of the A2 grain boundary showing four preparation sites for APT tips, the TEM thin foil was extracted close to these sites (in yellow), (c) STEM-HAADF image of the entire thin foil where the grain boundary is straight and close to the center of the sample.

The STEM-EDX analysis was performed using a FEI Tecnai OSIRIS equipped with the SuperX EDX system using four windowless detectors and operating at 200 kV. A thickness map at the grain boundary was acquired using energy filtered TEM by Gatan DigitalMicrograph3 [26] to determine the thickness at each STEM-EDX acquisition location and calculate the Absorption Correction Factor (ACF). A double tilt/rotation TEM sample holder was used to align the grain boundary parallel to the eucentric tilt axis. Next, the tilt was adjusted to vertically align the grain boundary, i.e. parallel to the primary electron beam. STEM-EDX acquisitions were performed using Esprit v1.9 developed by Bruker. The setting of the beam was done to obtain a beam current of 0.5 nA and a beam size of about 1 nm. With the thin foil thickness at approximately 100 nm, this beam

condition results at about 30 kcps during acquisition. Acquisition was performed using the hypermap function that maps a chosen area as shown in Figure 2 (a): an acquisition area (white dashed box) was selected based on a STEM Bright Field (BF) image. Mapping size is approximately 161 x 50 nm, giving a pixel size of 0.157 nm. Note that a pixel size much smaller than the beam size was deliberately chosen. Acquisition time is usually around 20 to 30 minutes for the entire map. The drift correction option in Esprit was used. The average drift observed during acquisition was approximately 30 nm. Figure 2 (b) shows the qualitative element maps (Fe Kα, P Kα) and the HAADF image of the acquisition zone. Phosphorus grain boundary segregation is clearly seen in the P Kα element map.

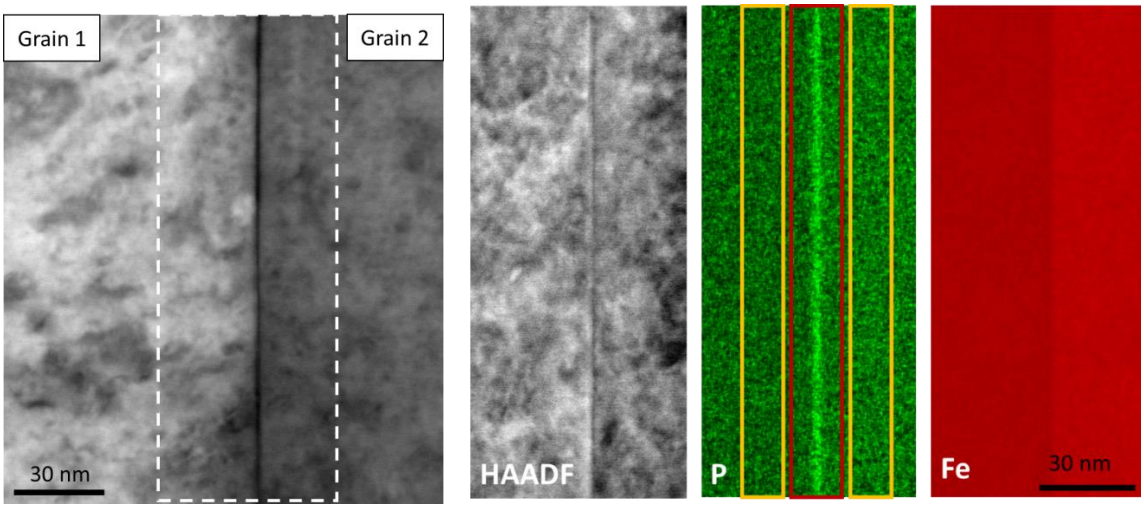

(a) (b)

Figure 2: Example of STEM-EDX acquisition on a Fe-P model alloy grain boundary: (a) STEM BF image of the thin foil with the EDX acquisition zone marked in white, (b) STEM HAADF image and EDX qualitative Fe Kα and P Kα maps, the red and yellow boxes indicate the zones considered for spectrum extraction during data processing.

Studies have shown that electron channeling, occurring when the electron beam is parallel to particular zone axes, can affect the EDX quantification [27], [28]. However, Lugg et al. [27] showed that once the electron beam is 2° off zone axis, the channeling effect is negligible. It has been

verified in this study that grain orientations were not under strong channeling conditions, so that negligible effect on the EDX quantifications is expected.

Data processing was conducted as follows. First, the sum spectra corresponding to three boxes of known width were extracted (Figure 2 (b)). The central red box was centered on the grain boundary and the two other yellow boxes were located in each adjacent grain. Figure 3(a) compares the "GB" spectrum (central box) and the "grain" spectrum (the two yellow boxes), where X-ray intensity is expressed in number of counts per second (cps). The grain spectrum $S_{Grain}$is obtained from:

$$S_{Grain} = \frac{B_1 + B_2}{t_1 + t_2} \quad (1)$$

where B_1 and B_2 are the "Grain1" and "Grain2" box spectra (yellow boxes in Figure 2(b)) expressed in raw counts, t_1 and t_2 are the counting times corresponding to "Grain1" and "Grain2" boxes (i.e. number of pixels in the box multiplied by the counting time per pixel). In Figure 3(a), the signal is expressed in counts per seconds to directly compare the "grain" and "GB" spectra.

The phosphorus peak on the grain boundary spectrum is clearly evidenced, see Figure 3(b). A small amount of sulfur grain boundary segregation was also detected, but this is not discussed in this work. The background shape and the presence of spurious peaks will be discussed later. The net phosphorus Kα peak was obtained by subtracting the grain spectrum from the GB spectrum (Figure 3(c)). A Gaussian function was fitted to the peak to determine phosphorus peak intensity (peak area, I_P in Eq (6)). Iron peak intensity (I_{Fe} in Eq (6)) was obtained in the same manner by fitting a Gaussian function to the iron Kα peak directly on the GB spectrum (Figure 3 (d)).

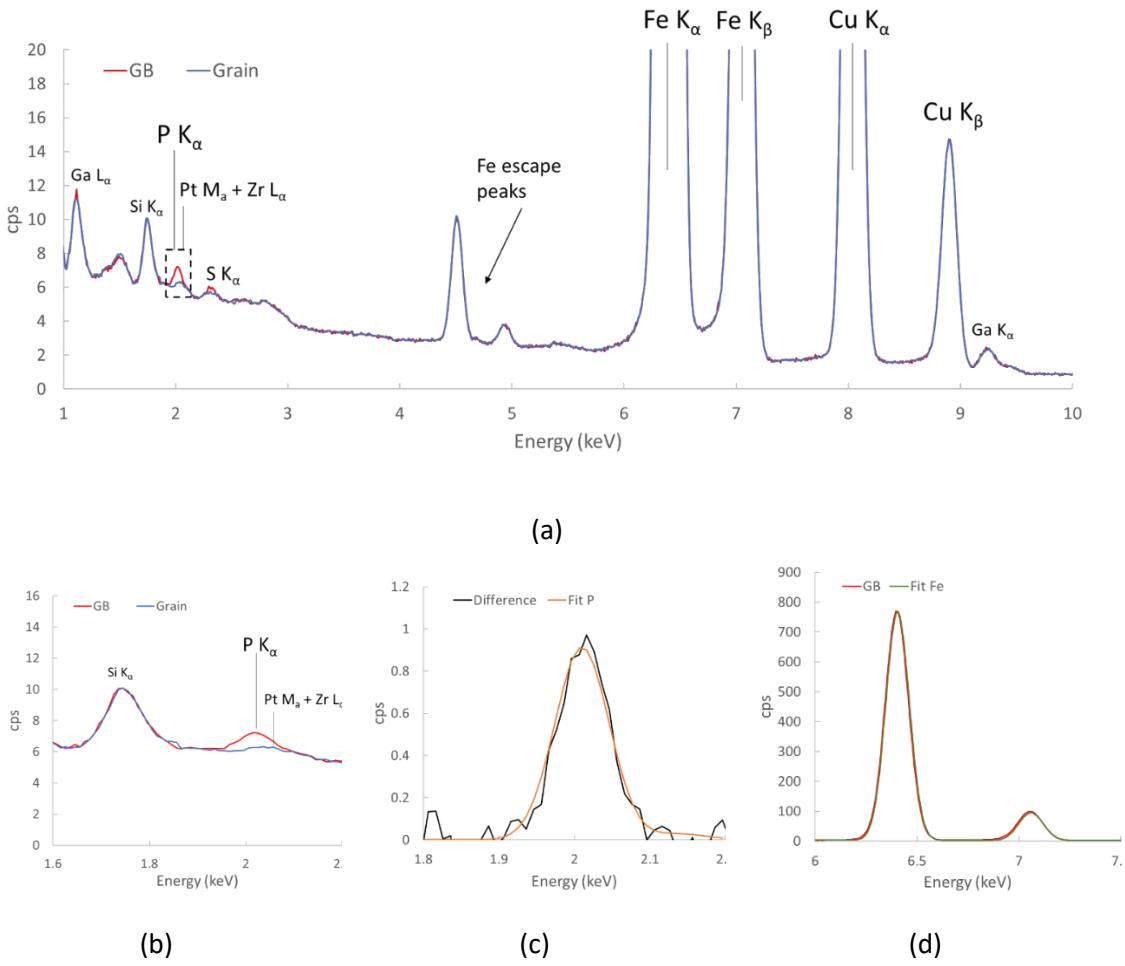

Figure 3: Example of STEM-EDX data processing on a Fe-P model alloy grain boundary: (a) superposed GB spectrum (corresponding to the red box in Figure 2(b)) and grain spectrum (corresponding to the two yellow boxes in Figure 2(b)), (b) zoom on (a) at the energy range close to the P Kα peak, (c) the P Kα peak after subtraction (GB spectrum minus Grain spectrum) fitted by a Gaussian function, (d) the Fe Kα and Fe Kβ peaks from the GB spectrum (corresponding to the red box in Figure 2(b)) fitted by a Gaussian function.

The Cliff-Lorimer method [29], also known as the k factor method was used for quantification.

The formula adapted to this study can be written as:

$$\frac{C_P}{C_{Fe}} = k_{P/Fe} * ACF_{\mathrm{P/Fe}} * \frac{I_P}{I_{Fe}} \qquad (2)$$

$$C_P + C_{Fe} = 1 \quad (3)$$

where $\frac{C_P}{C_{Fe}}$ is the composition ratio in wt% of the two elements P and Fe in the GB box, $k_{P/Fe}$ is the k factor of phosphorus with respect to iron, $ACF_{\mathrm{P/Fe}}$ is the absorption correction factor of phosphorus with respect to iron, and $\frac{I_P}{I_{Fe}}$ is the intensity ratio of the P Kα and Fe Kα peaks obtained in the GB box. The k factor was determined as 0.79 using an iron phosphide standard sample. It was determined by the parameterless extrapolation method proposed by Van Cappellen et al. [30] (see Appendix 1). The ACF of each X-ray line (P Kα and Fe Kα) was calculated based on the following equation [31]:

$$ACF = \frac{\frac{\mu}{\rho}\,\rho t\,\csc(\alpha)}{1 - \exp\left(-\frac{\mu}{\rho}\,\rho t\,\csc(\alpha)\right)} \quad (4)$$

Where $\frac{\mu}{\rho}$ is the mass absorption coefficient in cm/g based on the database of Chantler et al. [32], accessed by Hyperspy [33] (1474.48 cm/g for P Kα and 65.40 cm/g for Fe Kα respectively in the FeP model alloy), ρ is the density of the sample taken at 7.9 g/cm^3, t is the foil thickness at the acquisition location in cm, α is the take-off angle in radian, and csc is the cosecant function. The nominal take-off angle is designed to be 22° in the superX configuration; this value is taken as an approximation for all four detectors assuming the thin foil tilt is negligible. A nominal take-off angle is considered for the four detectors, as the individual counts per detector are inaccessible [34].

Once the ACF was determined for each X-ray line, $ACF_{\mathrm{P/Fe}}$ was obtained using:

$$ACF_{P/Fe} = \frac{ACF_P}{ACF_{Fe}} \quad (5)$$

From equations (2) and (3), we obtain C_P in wt%:

$$C_P = \frac{k_{P/Fe} * ACF_{\mathrm{P/Fe}} * \frac{I_P}{I_{Fe}}}{1 + k_{P/Fe} * ACF_{\mathrm{P/Fe}} * \frac{I_P}{I_{Fe}}} \quad (6)$$

The phosphorus grain boundary concentration was obtained using (adapted from [4]):

$$X_P = \frac{V}{A} N \frac{A_{Fe}}{A_P} C_P = wN \frac{A_{Fe}}{A_P} C_P \quad (7)$$

Where X_P is the phosphorus grain boundary concentration in atom/nm^2, N is the matrix density in nm^{-3} (85.49 nm^{-3} for iron), A_{Fe} and A_P are the atomic mass of iron and phosphorus, respectively. $\frac{V}{A}$ is the geometry factor, which is the ratio of the interaction volume to the area of the grain boundary. The raster scan approach in [4], [6] was used in this study. This simplifies the geometry factor ($\frac{V}{A}$) into the width *w* perpendicular to the grain boundary plane; therefore the grain boundary box width is used for *w* in Eq. (7).

3. Results and discussion

Multiple STEM-EDX acquisitions were performed along the grain boundary on each thin foil. Table 1 shows the data acquired on the two grain boundaries analyzed in this work and the quantification results. Fourteen acquisitions were conducted on A1 and ten were conducted on A2. The results obtained in [2], [25] using APT on the same two grain boundaries are also provided for comparison. A fair agreement is found between the two techniques, although the STEM-EDX quantification is slightly higher than that by APT; for grain boundary A1, the difference falls into the range of the standard deviation of the STEM-EDX measurement series.

Table 1: Phosphorus intergranular segregation quantification results by STEM-EDX compared with APT results from [2], [25] for two model Fe-P alloy grain boundaries. (1): Acquisitions #3 and #4 were conducted at the same location. (2): Acquisition from #11 to #14 were conducted six months later than acquisitions from #1 to #10.

GB	#	P peak intensity in the GB box (cps)	Fe peak intensity in the GB box (cps)	k factor ($k_{P/Fe}$)	Local thickness (nm)	$ACF_{P/Fe}$	P concentration in GB box (wt%)	GB box width (nm)	P concentration in GB box (atom/nm²)	P concentration by APT (atom/nm²)
A1	1	0.114	110.5	0.79	110	1.17	0.104%	11.8	1.89	
	2	0.110	103.2		110	1.17	0.109%	13.2	2.22	
	3(1)	0.092	84.8		160	1.25	0.117%	12.7	2.30	
	4(1)	0.098	84.6		160	1.25	0.125%	12.6	2.42	
	5	0.078	84.2		160	1.25	0.100%	11.3	1.75	
	6	0.147	87.8		160	1.25	0.181%	10.1	2.80	
	7	0.060	89.9		160	1.25	0.072%	12.9	1.43	
	8	0.112	92.0		160	1.25	0.132%	12.7	2.58	
	9	0.099	92.2		160	1.25	0.116%	12.4	2.23	
	10	0.099	94.0		160	1.25	0.114%	11.8	2.07	
	11(2)	0.054	64.8		140	1.22	0.088%	14.0	1.91	
	12(2)	0.054	74.4		140	1.22	0.077%	14.8	1.75	
	13(2)	0.067	87.6		140	1.22	0.081%	14.0	1.74	
	14(2)	0.042	77.8		140	1.22	0.057%	19.3	1.70	
	Average								2.06 ± 0.38	1.7 ± 0.35
A2	1	0.043	53.0	0.79	100	1.15	0.080%	23.9	2.95	
	2	0.084	103.1		100	1.15	0.081%	22.0	2.75	
	3	0.096	111.5		100	1.15	0.086%	20.3	2.69	
	4	0.096	131.2		90	1.14	0.072%	20.9	2.32	
	5	0.103	133.1		90	1.14	0.076%	23.4	2.73	
	6	0.098	144.5		90	1.14	0.067%	23.1	2.37	
	7	0.078	107.9		90	1.14	0.071%	22.5	2.45	
	8	0.069	103.1		90	1.14	0.066%	23.1	2.33	
	9	0.085	123.8		80	1.12	0.067%	26.4	2.75	
	10	0.085	111.4		80	1.12	0.075%	25.6	2.96	
	Average								2.63 ± 0.24	2.2 ± 0.17

3.1 Validation of the box method using Monte-Carlo simulation

Monte-Carlo simulations of electron beam scattering and X-ray emission were carried out using the MC X-ray program [35]. The objective was to ensure that the quantification method applied in this study was valid and not influenced by the beam-sample interaction volume. The effect of beam diameter and beam broadening due to sample thickness were studied. The program first allows the user to create a specimen geometry. Here, an iron thin foil containing a vertical "grain boundary" was created. The "grain boundary" is mimicked by a 0.2 nm thick Fe-P alloy layer of 7.86 g/cm^3 in density containing 6.5452 wt% of phosphorus, which corresponds to 2 atom/nm^2 of phosphorus.

During simulation, the program calculates X-ray intensities (P-Kα, Fe-Kα, Fe-Lα, etc.) at different beam locations. Beam movement (step size and number) is specified by the user. In this study, line profiles across the grain boundary were simulated. The primary beam energy was set to 200 keV. The electron beam shape was considered of Gaussian type. The beam diameter was defined as that containing 99.9% of the total number of electrons [35], [36]. The chosen number of electron trajectories simulated was high enough to keep statistical noise below approximately 1% of the peak height obtained on the X-ray line profiles obtained. The different physical models used for Monte-Carlo simulations were those set by default in the program [35].

The simulated P-Kα and Fe-Kα peak intensities were processed in the same manner as the experimental ones, i.e. using the Cliff-Lorimer equation to obtain local apparent phosphorus concentrations. The k factor of the Cliff-Lorimer method can be easily obtained by simulating X-ray intensities on a standard homogeneous specimen of known composition. If the standard specimen has the same thickness as the specimen of interest, no correction is required. Table 2 shows the k-factor determined using a homogeneous thin foil of Fe-1 wt %P with three

thicknesses. These k-factors values were then used to process the X-ray intensities obtained from the simulations, i.e. by converting them into phosphorus apparent concentrations.

Table 2: k factor (P in respect to Fe) calculated using Monte-Carlo simulation on a Fe-1 wt%P sample.

Thickness	Simulated k factor
50 nm	0.71
100 nm	0.76
150 nm	0.81

Figure 4 shows the calculated phosphorus concentration line profiles across the grain boundary for three beam diameters with a specimen thickness of 100 nm. The simulated phosphorus concentration was expressed as a weight fraction (left axis) and converted into a number of phosphorus atoms per unit volume (right axis). As expected, beam size affects the width of the concentration peak but does not change the area under peak: values of 1.99, 2.00 and 2.00 atom/nm^2 were obtained, corresponding to the input value of 2 atom/nm^2 specified in the specimen geometry. Line profiles rather than maps were simulated here to keep the simulation time reasonable (a few minutes per profile). In addition, this procedure also allows us to easily see how the concentration profile is affected when beam or specimen conditions are changed. However, calculation of the phosphorus interface concentration (2 atom/nm^2) from profile peak integration is strictly equivalent, from a mathematical point of view, to the “box-type” method employed to process experimental data (see Eq. (7)), provided that the box chosen is wide enough to include the entire phosphorus concentration peak.

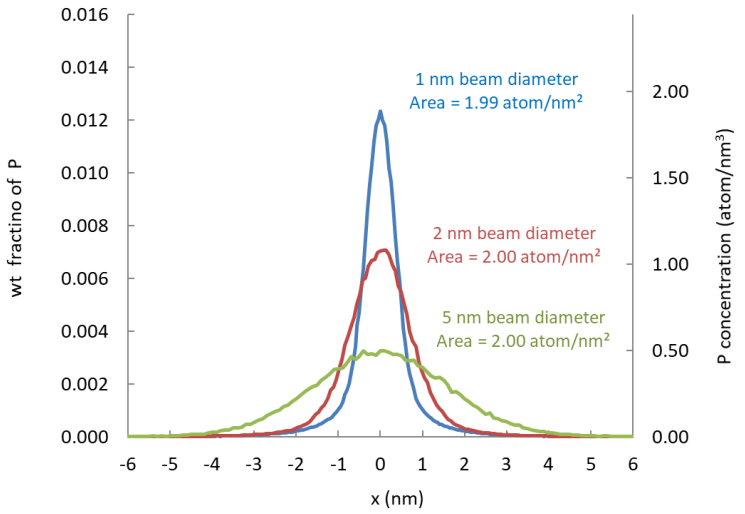

Figure 4: Beam size effect. Phosphorus concentration line profiles across the grain boundary calculated using Monte-Carlo simulation for three different beam diameters (sample thickness = 100 nm). The areas under peak are the same regardless of beam diameter and correspond to the input phosphorus grain boundary concentration of 2 atom/nm².

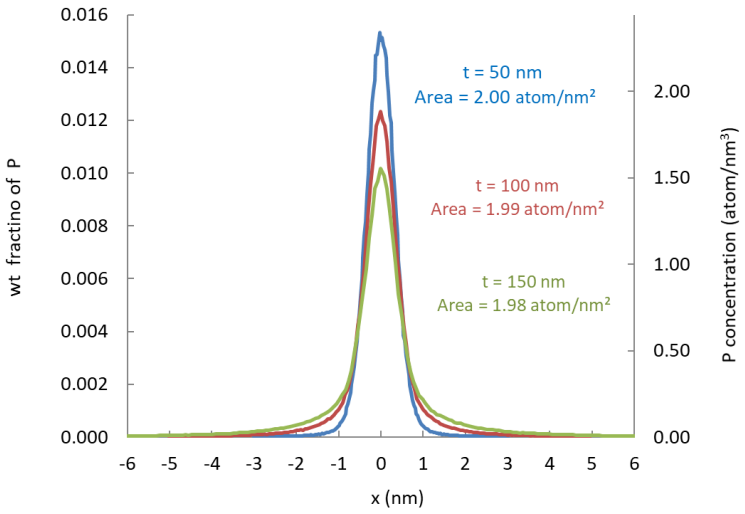

Figure 5: Thickness/beam broadening effect. Phosphorus concentration line profiles across the grain boundary calculated using the Monte-Carlo simulation for three thin foil thicknesses (beam diameter = 1 nm). The areas under peak are the same regardless of the beam broadening effect and correspond to an input phosphorus grain boundary concentration of 2 atom/nm².

Figure 5 shows the calculated phosphorus concentration line profiles across the grain boundary for three specimen thicknesses: 50, 100, and 150 nm. The beam diameter was set at 1 nm. It can be seen that the effect is similar to that of changing the beam diameter: peak height decreases but peak width increases with foil thickness. However, the peak area remains unchanged: 2.00, 1.99, and 1.98 atom/nm^2 are obtained, which again corresponds to the input value. This shows that beam broadening does not affect the quantification result if the GB box width (w in Eq. (7)) considered is large enough to include the entire phosphorus concentration peak. From a mathematical point of view, the unchanged peak area can be explained by the concept of convolution. The apparent phosphorus concentration profile is the convolution of the actual phosphorus concentration profile (practically a Dirac peak) with a normalized probe function [37]. From the properties of the convolution product, it was shown by Risch et al. [37] that the under-peak area of the apparent concentration profile does not depend on the shape of the probe function and always equals the under-peak area of the actual concentration profile (here 2 atom/nm^2).

Figure 6 provides a schematic of the beam broadening effect. Two cases (dashed line and continuous line) are presented: in the dashed line case, the beam is enlarged since the thin foil is thicker. The phosphorus signal starts to increase as the edge of the enlarged beam reaches the grain boundary. The dashed profile (thick foil case) starts to increase before the continuous profile (thin foil case). As the electron beam scans through the grain boundary, the dashed profile is broader and presents a lower peak height than the continuous profile. This is due to the larger interaction volume for the thick foil case. However, the area under peak should remain constant as shown by the simulation (Figure 5). This schematic also shows that the base peak width (w_P, width at C ≈ 0) is twice the maximum beam diameter, i.e. the beam diameter at the exit side of

the thin foil (d_B). In the box quantification method, the GB box width should be at least wider than w_P to include the entire grain boundary phosphorus signal.

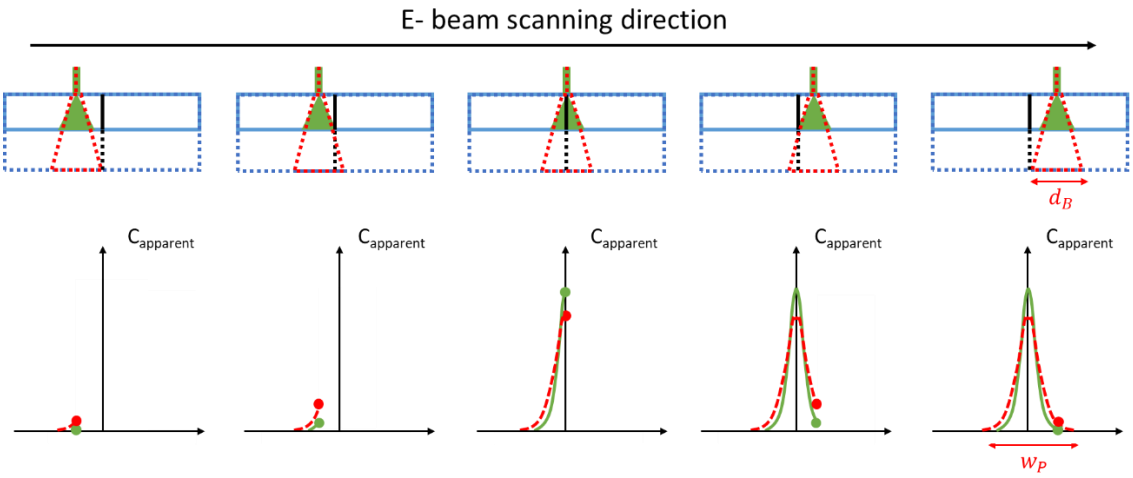

Figure 6: Schematic of an electron beam scanning through a sample with a grain boundary parallel to the electron beam. Two cases are presented: a thin sample (continuous line) and a thick sample (dashed line).

Figure 4, Figure 5 and Figure 6 show that once the GB box width (*w* in eq (7)) exceeds twice the broadened beam diameter, interaction volume and beam broadening have no more effect. In practice, box width is always chosen wider than the phosphorus-enriched region in the element map, see red box in Figure 2(b). The values of the box widths of different acquisitions are provided in Table 1 and are always wider than 10 nm. Under the acquisition condition defined (beam diameter around 1 nm, thin foil thickness ~100 nm), the "box" method applied allows the beam broadening effect to be ignored. Figure 7 shows quantification evolution depending on the grain boundary box width on one of the acquisitions on A2 grain boundary. When the box is too small, phosphorus concentration is underestimated as the GB spectrum does not contain all the segregation signals. As the box width increases, quantification begins to stabilize once it exceeds

5 nm. From this point, quantification is no longer dependent on box width. The black dot in Figure 7 is the value provided in Table 1.

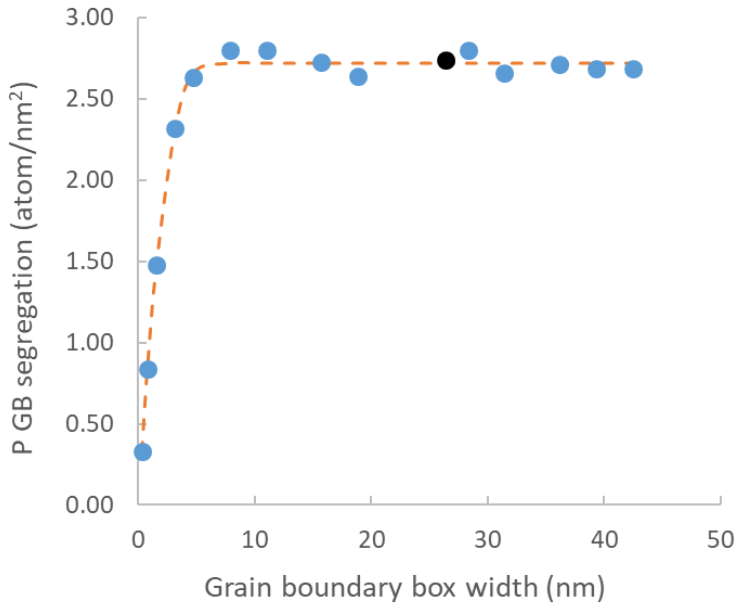

Figure 7: Box method data processing with different GB box widths based on a single acquisition on A2 grain boundary. The P concentration is underestimated when the GB box is too small, then it stabilizes once the box width reaches approximately 5 nm. Once the box width exceeds this stable point, it becomes irrelevant to the result. The black dot is the quantification provided in Table 1.

3.2 Validation of the background subtraction method

The background subtraction approach in this study was based on subtracting the average backgrounds of both adjacent grains. The main advantage of this method is to remove the effects of coherent Bremsstrahlung and possible spurious peaks. Figure 8 shows two spectra from each of the adjacent grains (the yellow boxes in Figure 2(b)). The shapes of the two spectra are very different at low energy (1 – 3.5 keV). The wavy shape of the background is due to coherent Bremsstrahlung [23]. According to [23], the positions of coherent Bremsstrahlung peaks are

related to crystal orientation. It was indeed verified in this study that coherent Bremsstrahlung is the same within the same grain, but differs from one grain to another (see Appendix 2).

Apart from the different background shapes, there are different spurious peaks present in the acquired spectra (see Figure 3(a) and Figure 8): Cu due to sample grid, Pt and Ga due to FIB preparation, Si and Zr due to SuperX detectors [24]. Some spurious peaks (Ga L series, Si Kα, Cu Kα) can be disregarded as they are far away from the phosphorus peak that is of interest here, and do not influence data processing. However, others (Zr Lα and Pt Mα) are very close to the phosphorus peak and cause difficulties in identification and quantification; see Figure 3(b).

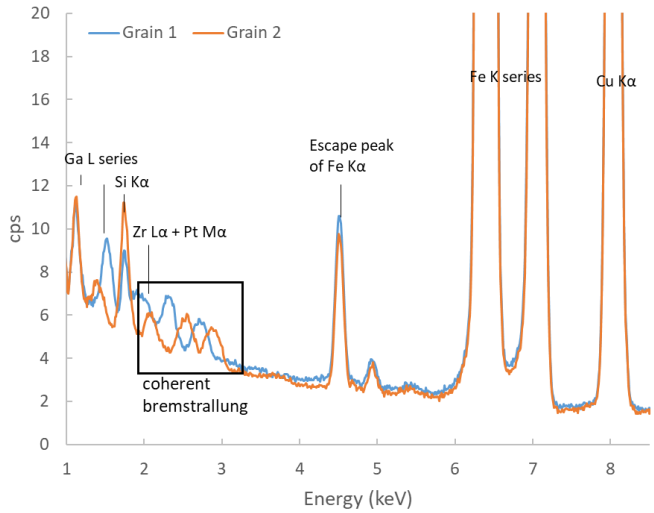

Figure 8: Spectra of the two adjacent grains of grain boundary A2 from the Fe-P model alloy showing coherent Bremsstrahlung at low energy (1 – 3.5 keV) and several spurious peaks. The spurious peaks of Pt and Zr are close to 2 keV and cannot be identified clearly because of the presence of coherent Bremsstrahlung.

All the artefacts above considerably increase the difficulty of accurate determination of phosphorus peak intensity from the grain boundary box spectrum. Obviously, common background subtraction methods are not applicable to this work. As such, it was decided to determine phosphorus peak intensity by subtracting the average spectrum of both the adjacent

grains. For this, the grain boundary box spectrum (red box in Figure 2(b)) must be "symmetrical". In other words, the grain boundary must be at the center of the GB box to ensure that the two adjacent grains contribute equally in the grain boundary spectrum. However, the two grain box spectra (yellow boxes in Figure 2(b) do not necessarily need to be the same size when expressed in cps as in Figure 3. Figure 3(a) shows that, when the grain and grain boundary spectra are superposed, the two backgrounds match nicely and the peaks of the segregated elements can be evidenced.

3.3 Measurement accuracy

The errors that are induced in this methodology can be categorized as random errors and systematic errors. The main source of *random* errors is the measurement of phosphorus peak intensity as iron peak intensity is higher by approximately a factor of 10^3 (Table 1). The relative counting error (68% confidence interval) is given by [23]:

$$\frac{\Delta X_P}{X_P} \cong \frac{\Delta I_P}{I_P} \cong \frac{\sqrt{N_T}}{N_P} \qquad (8)$$

where X_P is the phosphorus grain boundary concentration, I_P is the phosphorus peak intensity, N_T is the total number of counts in the P energy window (1.9 – 2.2 keV), and N_P is the number of counts in the P peak. Table 3 shows the counting data and counting error for each measurement conducted in this study. The relative counting error lies approximately between 5% and 10%.

Table 3: Counting data and relative counting errors for each measurement on the two Fe-P model alloy grain boundaries.

GB	#	N_P (counts)	N_T (counts)	$\frac{\Delta X_P}{X_P}$	$X_P \pm \Delta X_P$ (atom/nm^2)	
A1	1	9,319	299,812	0.059	1.67	0.10
	2	11,664	358,366	0.051	1.97	0.10
	3	7,495	193,388	0.059	2.03	0.12
	4	7,893	190,412	0.055	2.14	0.12
	5	5,666	171,306	0.073	1.55	0.11
	6	9,457	158,646	0.042	2.47	0.10
	7	4,951	206,843	0.092	1.27	0.12
	8	10,271	234,225	0.047	2.28	0.11
	9	7,902	203,908	0.057	1.97	0.11
	10	7,496	196,009	0.059	1.83	0.11
	11	4,377	175,101	0.096	1.68	0.16
	12	5,778	270,836	0.090	1.55	0.14
	13	10,801	415,777	0.060	1.54	0.09
	14	4,760	249,456	0.105	1.50	0.16
A2	1	3,536	138,406	0.105	2.60	0.27
	2	4,254	169,346	0.097	2.43	0.24
	3	5,050	189,048	0.086	2.37	0.20
	4	5,107	216,124	0.091	2.05	0.19
	5	10,322	406,255	0.062	2.41	0.15
	6	9,793	430,973	0.067	2.10	0.14
	7	6,825	278,722	0.077	2.17	0.17
	8	5,016	223,811	0.094	2.06	0.19
	9	5,701	234,707	0.085	2.43	0.21
	10	4,683	176,974	0.090	2.61	0.23

It should be noted that, for A2 grain boundary, the calculated counting errors (0.14 to 0.27 atom/nm^2) are in good agreement with the standard deviation (0.21 atom/nm^2) of the series of measurements. For A1 grain boundary, however, the standard deviation (0.34 atom/nm^2) of the

series of measurements is significantly higher than the counting error (0.09 to 0.16 atom/nm^2). This suggests, for A1 grain boundary, an additional source of variability, possibly a non-homogeneous P concentration along the grain boundary [20].

A possible source of *systematic* error is the foil thickness used in ACF determination. Local foil thickness is measured using the thickness map function proposed by Gatan DigitalMicrograph3 [26]. It consists of measuring the thickness over the inelastic mean free path ($\frac{t}{\lambda}$), where the mean free path is estimated at 102 nm for pure iron [38]. Using this method, it is reasonable to estimate a 15% error in the foil thickness measurement. However, in the thickness range covered in this work (mainly 100 – 150 nm, see Table 1), ± 15% error in thickness measurement only results in ± 2.5% in the final P grain boundary segregation quantification. Another possible source of systematic error is the $k_{P/Fe}$ constant. However, in this work, as this constant was experimentally determined on a standard material in the same conditions as P grain boundary segregation measurements (see Appendix 1), this error is expected to be low.

3.4 Influence of electron dose and specimen ageing

It can be questioned whether the highly accelerated electrons used in TEM could result in irradiation damage in the segregated layer (knock out of P atoms) and hence decrease the amount of segregated solute. To check whether this effect could occur in our analyses, two acquisitions (#3 and #4 in Table 1) were conducted the same day at the same location (within nanometer positioning error due to specimen positioning and/or beam drift during acquisition). It can be seen that the phosphorus concentrations measured are not very different, which shows that there was no significant effect of the electron dose received during acquisition on the phosphorus grain boundary concentration, at least in the conditions of measurement used in this work.

In addition, it can also be questioned if storing the specimen for long time at room temperature before analysis could affect the amount of solute segregated at the grain boundary. To answer that question, acquisitions #11 to #14 on grain boundary A1 were conducted six months later than acquisitions #1 to #10. In the meanwhile, the thin foil was stored under vacuum at ambient temperature. The P concentration measured for acquisitions #11 to #14 are slightly lower than the previous acquisitions #1-#10, which might show that a small amount of phosphorus has migrated out of the grain boundary. However, the decrease observed is only slightly above the measurement accuracy. This shows that the specimen can be safely stored at room temperature before analysis, a least for weeks.

4 Conclusion

This study provides a method to quantify phosphorus grain boundary segregation using STEM-EDX. The ongoing consideration of beam/sample interaction volume and beam broadening effect can be ignored using the box spectrum method coupled with EDX mapping, provided the chosen GB box is wide enough ($w > w_P = 2d_B$). A novel background subtraction method, considering the equal contribution of adjacent grains in the GB box, is proposed. This removes the Bremsstrahlung background, the effect of coherent Bremsstrahlung, and spurious peaks present in the spectra. The method developed was applied to two high angle grain boundaries in iron containing about 2 atoms of phosphorus per nm². The quantitative results obtained are in good agreement with previous measurements conducted on the same two grain boundaries using APT, which suggests that the STEM-EDX box spectrum method can provide accurate measurements for grain boundary segregation.

5 Acknowledgement

We would like to acknowledge A. Akhatova who provided us with all the information we required and a sample of the model Fe-P alloy.

6 Funding

This research was mainly funded by EDF (Electricité de France) with the support of ANRT (Association Nationale de la Recherche et de la Technologie).

7 References

[1] F. Christien, R. [Le Gall, and G. Saindrenan, "Phosphorus grain boundary segregation in steel 17-4PH," *Scripta Materialia*, vol. 48, no. 1, pp. 11–16, 2003, doi: https://doi.org/10.1016/S1359-6462(02)00309-3.

[2] A. Akhatova *et al.*, "Investigation of the dependence of phosphorus segregation on grain boundary structure in Fe-P-C alloy: cross comparison between Atom Probe Tomography and Auger Electron Spectroscopy," *Applied Surface Science*, vol. 463, pp. 203–210, Jan. 2019, doi: 10.1016/j.apsusc.2018.08.085.

[3] L. Zhang, B. Radiguet, P. Todeschini, C. Domain, Y. Shen, and P. Pareige, "Investigation of solute segregation behavior using a correlative EBSD/TKD/APT methodology in a 16MND5 weld," *Journal of Nuclear Materials*, vol. 523, pp. 434–443, 2019, doi: https://doi.org/10.1016/j.jnucmat.2019.06.002.

[4] V. J. Keast and D. B. Williams, "Quantification of boundary segregation in the analytical electron microscope," *J Microsc*, vol. 199, no. 1, pp. 45–55, Jul. 2000, doi: 10.1046/j.1365-2818.2000.00694.x.

[5] T. Hu, S. Yang, N. Zhou, Y. Zhang, and J. Luo, "Role of disordered bipolar complexions on the sulfur embrittlement of nickel general grain boundaries," *Nat Commun*, vol. 9, no. 1, p. 2764, Dec. 2018, doi: 10.1038/s41467-018-05070-2.

[6] J. A. S. Ikeda, Y.-M. Chiang, A. J. Garratt-Reed, and J. B. V. Sande, "Space Charge Segregation at Grain Boundaries in Titanium Dioxide: II, Model Experiments," *Journal of the American Ceramic Society*, vol. 76, no. 10, pp. 2447–2459, 1993, doi: 10.1111/j.1151-2916.1993.tb03965.x.

[7] M. Watanabe, "Microscopy Hacks: development of various techniques to assist quantitative nanoanalysis and advanced electron microscopy," *Microscopy (Tokyo)*, vol. 62, no. 2, pp. 217–241, Apr. 2013, doi: 10.1093/jmicro/dfs085.

[8] U. Alber, H. Miillejans, and M. Riihle, "Improved quantification of grain boundary segregation by EDS in a dedicated STEM," p. 12, 1997.

[9] T. Walther, A. Rečnik, and N. Daneu, "A Novel Method of Analytical Transmission Electron Microscopy for Measuring Highly Accurately Segregation to Special Grain Boundaries or Planar Interfaces," *Microchimica Acta*, vol. 155, no. 1–2, pp. 313–318, Sep. 2006, doi: 10.1007/s00604-006-0562-5.

[10] X. F. Zhang, Q. Yang, L. C. De Jonghe, and Z. Zhang, "Energy dispersive spectroscopy analysis of aluminium segregation in silicon carbide grain boundaries," *J Microsc*, vol. 207, no. 1, pp. 58–68, Jul. 2002, doi: 10.1046/j.1365-2818.2002.01034.x.

[11] D. B. Williams and A. D. Romig, “Studies of interfacial segregation in the analytical electron microscope: A brief review,” *Ultramicroscopy*, vol. 30, no. 1, pp. 38–51, Jun. 1989, doi: 10.1016/0304-3991(89)90171-X.
[12] I. A. Vatter and J. M. Titchmarsh, “Measurement of grain-boundary segregation by STEM-EDX analysis,” *Ultramicroscopy*, vol. 28, no. 1, pp. 236–239, 1989, doi: https://doi.org/10.1016/0304-3991(89)90301-X.
[13] P. Doig, D. Lonsdale, and P. E. J. Flewitt, “Segregation of embrittling elements to prior austenite grain boundaries in 2·25Cr–1 Mo steel,” *Metal Science*, vol. 16, no. 7, pp. 335–344, Jul. 1982, doi: 10.1179/030634582790427488.
[14] R. G. Faulkner, S.-H. Song, and P. E. J. Flewitt, “Combined quenching and tempering induced phosphorus segregation to grain boundaries in 2-25Cr-1 Mo steel,” *Materials Science and Technology*, vol. 12, pp. 818–822, 1996, doi: 10.1179/mst.1996.12.10.818.
[15] P. Lejcek, *Grain boundary segregation in metals*. Berlin: Springer-Verlag, 2010.
[16] C. A. English, S. R. Ortner, G. Gage, W. L. Server, and S. T. Rosinski, “Review of Phosphorus Segregation and Intergranular Embrittlement in Reactor Pressure Vessel Steels”, doi: 10.1520/STP10531S.
[17] S.-G. Park, K.-H. Lee, M.-C. Kim, and B.-S. Lee, “Effects of boundary characteristics on resistance to temper embrittlement and segregation behavior of Ni–Cr–Mo low alloy steel,” *Materials Science and Engineering: A*, vol. 561, pp. 277–284, Jan. 2013, doi: 10.1016/j.msea.2012.10.078.
[18] S. Raoul, B. Marini, and A. Pineau, “Effect of microstructure on the susceptibility of a 533 steel to temper embrittlement,” *Journal of Nuclear Materials*, p. 7, 1998.
[19] S.-H. Song, Y. Zhao, Y. Cui, J. Sun, H. Si, and J.-Q. Li, “Effect of grain boundary character distribution and grain boundary phosphorus segregation on the brittleness of an interstitial-free steel,” *Materials Letters*, vol. 182, pp. 328–331, Nov. 2016, doi: 10.1016/j.matlet.2016.07.023.
[20] D.-D. Shen, S.-H. Song, Z.-X. Yuan, and L.-Q. Weng, “Effect of solute grain boundary segregation and hardness on the ductile-to-brittle transition for a Cr–Mo low-alloy steel,” *Materials Science and Engineering: A*, vol. 394, no. 1–2, pp. 53–59, Mar. 2005, doi: 10.1016/j.msea.2004.10.036.
[21] R. Ding and J. Knott, “Grain boundary segregation of phosphorus and molybdenum in 2·25Cr–1Mo steel,” *Materials Science and Technology*, vol. 24, no. 10, pp. 1189–1194, 2008, doi: 10.1179/174328407X157407.
[22] M. A. Islam, “Grain Boundary Segregation Behavior in 2.25Cr-1Mo Steel During Reversible Temper Embrittlement,” *J of Materi Eng and Perform*, vol. 16, no. 1, pp. 73–79, Feb. 2007, doi: 10.1007/s11665-006-9011-1.
[23] D. B. Williams and C. B. Carter, *Transmission electron microscopy: a textbook for materials science*, 2nd ed. New York: Springer, 2008.
[24] W. Grogger, S. Fladischer, J. Kraxner, M. Paller, and G. Kothleitner, “Quantitative EDXS: Influence of Detector Geometry,” presented at the Super X user meeting 2014, 2014.
[25] A. Akhatova, “Méthodologie instrumentale à l’échelle atomique pour une meilleure compréhension des mécanismes de ségrégation intergranulaire dans les aciers: application au phosphore.,” Université de Rouen, 2017.
[26] T. Malis, S. C. Cheng, and R. F. Egerton, “EELS log-ratio technique for specimen-thickness measurement in the TEM,” *Journal of Electron Microscopy Technique*, vol. 8, no. 2, pp. 193–200, Feb. 1988, doi: 10.1002/jemt.1060080206.

[27] N. R. Lugg, G. Kothleitner, N. Shibata, and Y. Ikuhara, “On the quantitativeness of EDS STEM,” *Ultramicroscopy*, vol. 151, pp. 150–159, Apr. 2015, doi: 10.1016/j.ultramic.2014.11.029.
[28] Z. Chen, A. J. D’Alfonso, M. Weyland, D. J. Taplin, L. J. Allen, and S. D. Findlay, “Energy dispersive X-ray analysis on an absolute scale in scanning transmission electron microscopy,” *Ultramicroscopy*, vol. 157, pp. 21–26, Oct. 2015, doi: 10.1016/j.ultramic.2015.05.010.
[29] G. Cliff and G. W. Lorimer, “The quantitative analysis of thin specimens,” *Journal of Microscopy*, vol. 103, no. 2, pp. 203–207, Mar. 1975, doi: 10.1111/j.1365-2818.1975.tb03895.x.
[30] E. Van Cappellen, “The parameterless correction method in X-ray microanalysis,” *Microscopy Microanalysis Microstructures*, vol. 1, no. 1, pp. 1–22, 1990, doi: 10.1051/mmm:01990001010100.
[31] J. Philibert, “A Method for Calculating the Absorption Correction in Electron-Probe Microanalysis,” in *X-ray Optics and X-ray Microanalysis*, Elsevier, 1963, pp. 379–392. doi: 10.1016/B978-1-4832-3322-2.50039-1.
[32] C. T. Chantler, “Detailed Tabulation of Atomic Form Factors, Photoelectric Absorption and Scattering Cross Section, and Mass Attenuation Coefficients in the Vicinity of Absorption Edges in the Soft X-Ray (Z=30–36, Z=60–89, E=0.1 keV–10 keV), Addressing Convergence Issues of Earlier Work,” *Journal of Physical and Chemical Reference Data*, vol. 29, no. 4, pp. 597–1056, Jul. 2000, doi: 10.1063/1.1321055.
[33] F. de la Pena *et al.*, *hyperspy/hyperspy v1.4.1*. 2018. doi: 10.5281/zenodo.1469364.
[34] J. Kraxner *et al.*, “Quantitative EDXS: Influence of geometry on a four detector system,” *Ultramicroscopy*, vol. 172, pp. 30–39, Jan. 2017, doi: 10.1016/j.ultramic.2016.10.005.
[35] P. Michaud and R. Gauvin, “MC X-Ray, The Monte Carlo Program for Quantitative Electron Microscopy of Real Materials,” *Microscopy and Microanalysis*, vol. 16, no. S2, pp. 278–279, 2010, doi: 10.1017/S1431927610054668.
[36] D. Drouin, A. R. Couture, D. Joly, X. Tastet, V. Aimez, and R. Gauvin, “CASINO V2.42—A Fast and Easy-to-use Modeling Tool for Scanning Electron Microscopy and Microanalysis Users,” *Scanning*, vol. 29, no. 3, pp. 92–101, May 2007, doi: 10.1002/sca.20000.
[37] F. Christien and P. Risch, “Cross-sectional measurement of grain boundary segregation using WDS,” *Ultramicroscopy*, vol. 170, pp. 107–112, Nov. 2016, doi: 10.1016/j.ultramic.2016.08.005.
[38] K. Iakoubovskii, K. Mitsuishi, Y. Nakayama, and K. Furuya, “Mean free path of inelastic electron scattering in elemental solids and oxides using transmission electron microscopy: Atomic number dependent oscillatory behavior,” *Phys. Rev. B*, vol. 77, no. 10, p. 104102, Mar. 2008, doi: 10.1103/PhysRevB.77.104102.
[39] P. J. Sheridan, “Determination of experimental and theoretical kASi factors for a 200-kV analytical electron microscope,” *Journal of Electron Microscopy Technique*, vol. 11, no. 1, pp. 41–61, Jan. 1989, doi: 10.1002/jemt.1060110107.

8 Appendix 1: Determination of the k factor and the absorption correction factor

In order to determine $k_{P/Fe}$, an iron phosphide sample was used as a standard material. Its composition was measured by Wavelength Dispersive X-ray Spectroscopy (WDS) at 58.37 wt% Fe and 29.22 wt% P. The total is not 100 wt% since there were trace amounts of other elements, such as manganese. Not all trace elements were identified as the determination of the $k_{P/Fe}$ factor is based on the P/Fe composition ratio only, therefore, the concentration of other elements was not required.

A wedge shaped FIB thin foil was extracted from the iron phosphide sample at the exact location where the WDS analysis was carried out. A map of the thin foil thickness was measured by energy filtered TEM using DigitalMicrograph3 by Gatan [26]. Then, a matrix of EDX acquisitions was constituted. Figure 9 shows an illustration of the wedge thin foil and the acquisition matrix.

Larger foil thickness results in higher X-ray emission as well as larger absorption. The EDX spectra obtained at different foil thicknesses were processed using the extrapolation method proposed by Van Cappellen [30], which determines the intensity ratio at zero foil thickness, i.e. free from absorption effect. The ratio of X-ray line intensities (I_P/I_{Fe}) is plotted versus the total intensity of X-ray lines (I_P+I_{Fe}) allowing the intensity ratio at zero thickness to be determined from the y-intercept (Figure 10). This procedure determines a $k_{P/Fe}$ factor at zero foil thickness, i.e. free from correction factors, using the following equation:

$$k_{P/Fe} = \frac{C_P}{C_{Fe}} * \frac{I_{Fe}}{I_P} = \frac{29.22}{58.37} * \frac{1}{0.6337} = 0.79 \quad (9)$$

The $k_{P/Fe}$ factor determined experimentally in this study is 0.79, which is very close to the one determined in [39] (0.77).

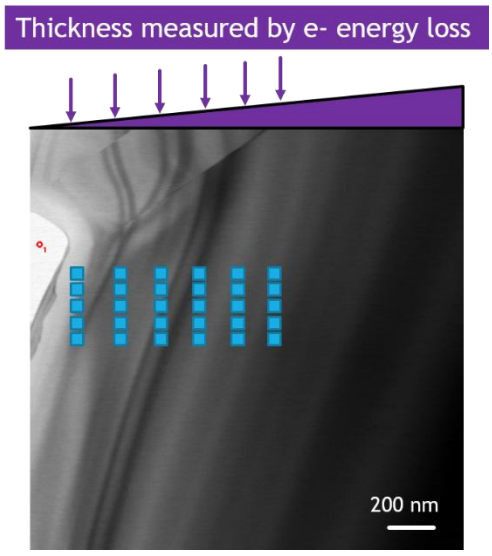

Figure 9: STEM BF image of the wedge shape thin foil of standard iron phosphide material. The blue boxes represent EDX acquisitions conducted at different thicknesses.

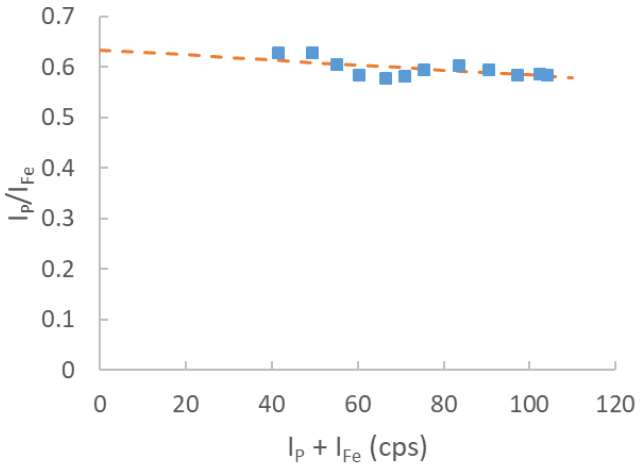

Figure 10: Parameterless extrapolation method of Van Cappellen [30] to determine the intensity ratio at zero foil thickness.

9 Appendix 2: Coherent Bremsstrahlung

Figure *11* shows two spectra from two different boxes of the same grain (grain 1 of A2 grain boundary). Exactly the same peaks of coherent Bremsstrahlung are obtained. On the other hand,

Figure 12 shows four spectra from the four different grains, corresponding to the two analyzed grain boundaries. Different coherent Bremsstrahlung peaks are obtained for each grain. Those observations are consistent with the fact that coherent Bremsstrahlung is related to crystal orientation [23].

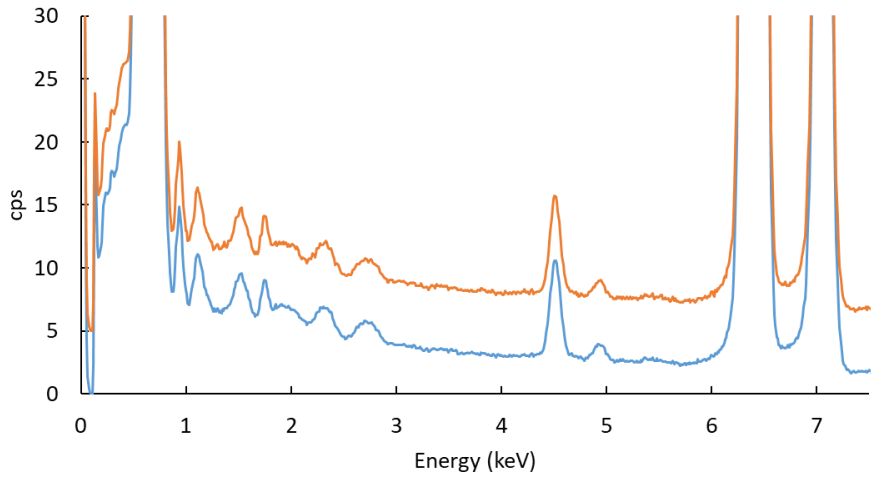

Figure 11: Spectra obtained from two different boxes of the same grain (grain one of GB A2). The two curves overlap completely. The orange curve is shifted 5 cps upwards for clarity.

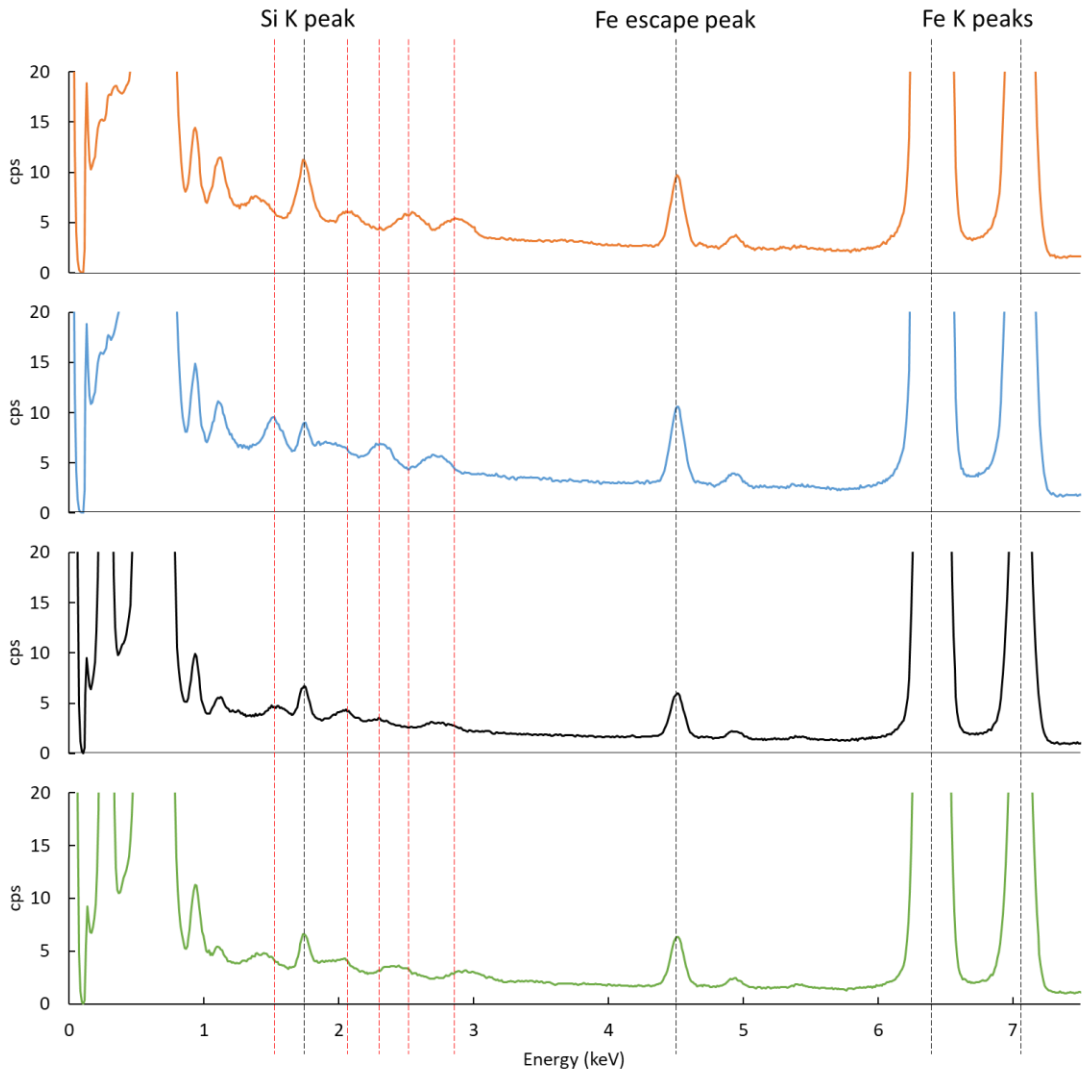

Figure 12: The four grain box spectra from the two analyzed grain boundaries. The black lines mark out the different element peaks that are at identical positions in all spectra. The red lines indicate different coherent Bremsstrahlung peaks from different grains.